J Mater Sci (2009) 44:2916–2924
DOI 10.1007/s10853-009-3385-z

High cycle fatigue behavior of as-extruded ZK60 magnesium alloy

W. C. Liu · J. Dong · P. Zhang · Z. Y. Yao · C. Q. Zhai · W. J. Ding

Received: 16 September 2008 / Accepted: 4 March 2009 / Published online: 25 March 2009

Abstract Tensile and high cycle fatigue properties of hot extruded ZK60 magnesium alloy have been investigated, in comparison to that of hot-extruded plus T5 heat-treated ZK60 magnesium alloy which was named as ZK60-T5. High cycle fatigue tests were carried out at a stress rate (R) of -1 and a frequency of 100 Hz using hour-glass-shaped round specimens with a gage diameter of 5.8 mm. The results show that tensile strength greatly improved and elongation is also slightly enhanced after T5 heat treatment, and the fatigue strength (at 10^7 cycles) of ZK60 magnesium alloy increases from 140 to 150 MPa after T5 heat treatment, i.e., the improvement of 7% in fatigue strength has been achieved. Results of microstructure observation suggest that improvement of mechanical properties of ZK60 magnesium alloy is due to precipitation strengthening phase and texture strengthening by T5 heat treatment. In addition, fatigue crack initiations of ZK60 and ZK60-T5 magnesium alloys were observed to occur from the specimen surface and crack propagation was characterized by striation-like features coupled with secondary cracks.

W. C. Liu · J. Dong (✉) · Z. Y. Yao · C. Q. Zhai · W. J. Ding
National Engineering Research Center of Light Alloy Net Forming, School of Materials Science and Engineering, Shanghai Jiao Tong University, Shanghai 200240, China
e-mail: jiedong@sjtu.edu.cn

W. C. Liu
e-mail: liuwc@sjtu.edu.cn

P. Zhang
Lehrstuhl Metallkunde und Werkstofftechnik, BTU-Cottbus, Postfach 101344, 03013 Cottbus, Germany

C. Q. Zhai · W. J. Ding
Key State Laboratory of Metal Matrix Composite, School of Materials Science and Engineering, Shanghai Jiao Tong University, Shanghai 200240, China

Introduction

Due to the increasing global energy demand and high consciousness of environmental protection in recent years, magnesium alloys are very attractive materials due to their low density, high specific strength and easily recycling compared to other metals and alloys. As low-weight structural materials, there has been significant increase in usage of magnesium alloy for automobile, aerospace components and other transportation industries [1–3]. Current major automotive magnesium applications are die castings including instrument panel beam, transfer case, transmission case, engine block, steering components, and radiator support. For the applications to the load-bearing components, it is necessary to understand the mechanical properties, in particular, fatigue properties of the magnesium alloys. There is some level of fatigue data of cast magnesium alloys available to the industry [4–6]. As magnesium is expanding into more critical applications in power-train, chassis and body areas, there is a great need for developing wrought magnesium products with improved mechanical properties including fatigue resistance.

As a wrought magnesium alloy, ZK60 has high tensile strength and excellent plasticity among commercial magnesium alloys [7]; its microstructure, mechanical properties, deformation treatment, and the effects of alloy elements and microelements are well studied [8]. At present, the researches on ZK60 magnesium alloy are mainly focused on plasticity, superplasticity [9] and ZK60-based composite [10]. However, the main property to determine the

application of ZK60 magnesium alloy in automotive industry is its tensile property, fatigue property and wear resistance [11, 12]. At present, only a limited study on the mechanical properties especially fatigue property of as-extruded ZK60 magnesium alloy has been reported in the literature [13–15]. This study was driven by the expansion of application of high strength wrought magnesium alloy ZK60. In this study, the tensile and high-cycle fatigue properties of hot-extruded magnesium alloy ZK60 were investigated in comparison to that of hot-extruded plus T5 heat-treated magnesium alloy ZK60 which was named as ZK60-T5.

Experimental

The magnesium alloy ZK60 (nominal composition in wt%: 5–6 Zn, 0.3–0.9 Zr, balance Mg) used in this study was produced by semi-continuous casting. Ingots of ZK60 magnesium alloy were prepared from high-purity Mg (99.95%), Zn (99.9%), and Mg–30Zr (wt%) master alloys in electric resistance furnace under the mixed atmosphere of CO_2 and SF_6 with the ratio of 100:1. When the temperature reached 760 °C, molten metal was stirred for about 5 min and held for 30 min, and then poured into steel molds of ∅ 100 mm × 350 mm held at approximately 200 °C. Analysis of the chemical composition of magnesium alloy ZK60 was done using Plasma-400, and results of chemical composition were shown in Table 1. The ingots were homogenized at 400 °C for 14 h. Then they were hot extruded to a cylindrical bar of 26.8 mm in diameter after soaking at 390 °C for 3 h, with an extrusion ratio of 14. T5 (150 °C/24 h) treatment was applied to some of the as-extruded bars.

Specimens for mechanical testing were machined with the load axis parallel to extrusion direction (ED) of the as-extruded bars. Tensile properties of ZK60 and ZK60-T5 magnesium alloys were performed with sheet specimens with marked dimension of 15-mm gauge length, 3.6-mm width and 2-mm thickness on Zwick/Roell Z020 tensile machine at room temperature.

For fatigue testing, hour-glass-shaped round specimens (see Fig. 1) were used; the dimensions of the specimens were as per the instruction of the ASTM E 466 specification with a gage diameter of 5.8 mm. The machined

Table 1 Chemical composition of magnesium alloy ZK60

Material	Composition (wt%)		
	Mg	Zn	Zr
ZK60 and ZK60-T5	Balance	5.54	0.56

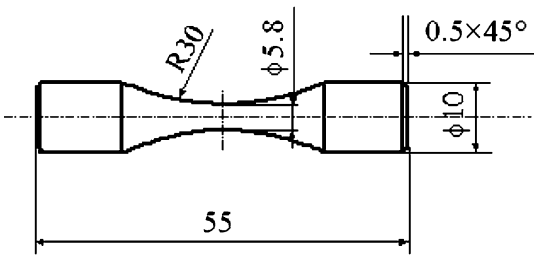

Fig. 1 Shape and size of hour-glass-shaped round specimen for fatigue test

specimens were electrolytically polished (EP) in order to avoid the influence of machining on the fatigue results.

Fatigue tests were performed under rotating beam loading ($R = -1$) at a frequency of about 100 Hz in air. The stress amplitude ranged from 90 to 260 MPa.

Phase composition and crystallographic texture were characterized by X-ray diffraction using Ni-filtered Cu Kα radiation. Crack initiation and propagation behaviors during fatigue were investigated by the replica method with a light optical microscope (LOM) at 400× magnification. Microstructure of the investigated alloys was also observed by LOM. Analyses of the chemical compositions of the microstructure, and the fracture surfaces after tensile and fatigue failure in ZK60 and ZK60-T5 magnesium alloys were done using scanning electron microscopy (SEM, Philip-505).

Results and discussion

Microstructure

Figure 2 shows the microstructures of ZK60 and ZK60-T5 in a plane parallel to the ED. As seen from Fig. 2a, the microstructure of ZK60 consists of banded microstructures of the dark region and surrounding light region that are typically characteristic of deformation structure, these regions appears as parallel layers [16, 17]. A schematic illustration is shown at the right side of the figure. Analysis of the composition of each layer was done using EDX analysis. Widths of the A, B and C compounds were measured using a LOM. Table 2 shows identifications of the phases of ZK60 and ZK60-T5 magnesium alloys by EDX analysis and LOM. In the table, the sizes of the layers are also listed. As seen from the table, the light layer (compound A) and the dark layer (compound C) observed in ZK60 magnesium alloy of Fig. 2a are 95.5Mg–3.4Zn–1.1Zr (at.%, primary α-Mg) and intermetallic phase of 64.1Mg–29.3Zn–6.3Zr (at.%) and α-Mg, respectively. The compound B is 89.8Mg–8.9Zn–1.3Zr (at.%). Average layer dimensions of the compounds, W_A, W_B and W_C are 22, 9

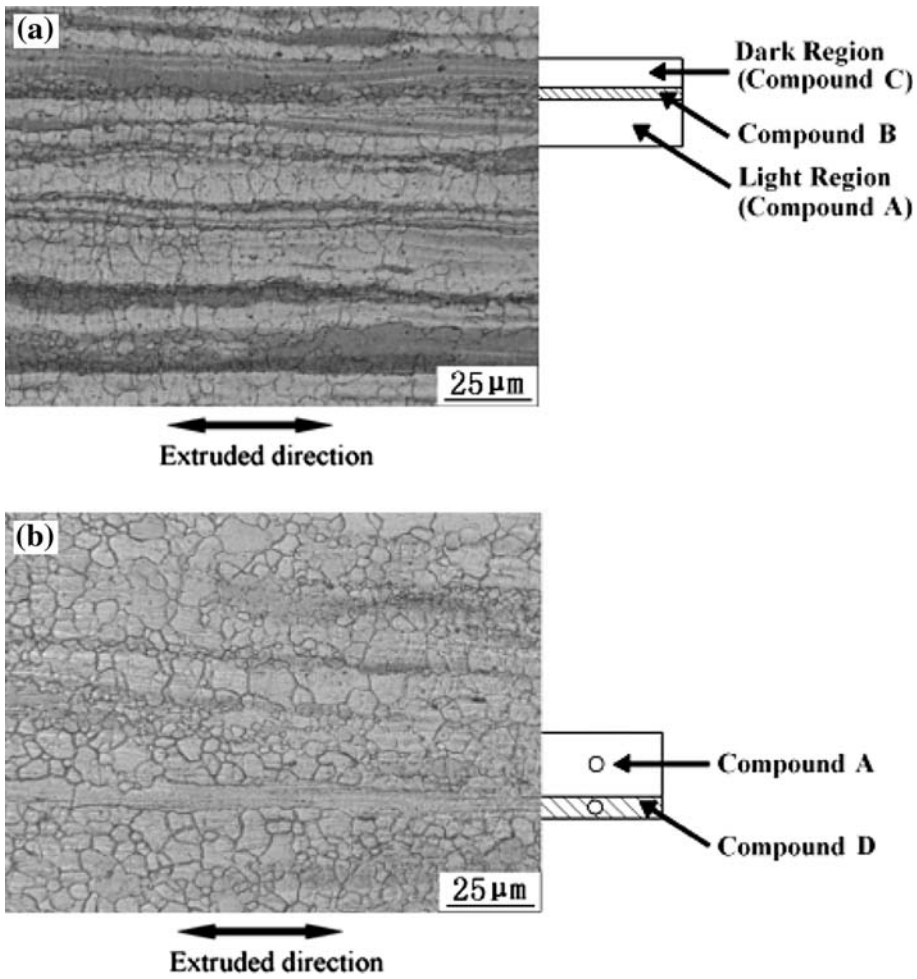

Fig. 2 Microstructure of the investigated alloys along extrusion direction: **a** ZK60; **b** ZK60-T5

Table 2 Compositions of the compounds in ZK60 and ZK60-T5

(a) Structure of ZK60	Composition (at.%)	Typical size (μm)
A	95.5Mg–3.4Zn–1.1Zr	$W_A = 22$
B	89.8Mg–8.9Zn–1.3Zr	$W_B = 9$
C	64.1Mg–29.3Zn–6.3Zr and α-Mg	$W_C = 16$
(b) Structure of ZK60-T5	Composition (at.%)	
A	95.5Mg–3.4Zn–1.1Zr	
D	54.8Mg–35.5Zn–9.7Zr and α-Mg	

and 16 μm, respectively, where W_A, W_B and W_C are width of the A, B and C compound, respectively. However, banded microstructures of ZK60 magnesium alloy are not clearly defined after T5 heat treatment (see Fig. 2b), its A and D compound are 95.5Mg–3.4Zn–1.1Zr (at.%, primary α-Mg) and intermetallic phase of 54.8Mg–35.5Zn–9.7Zr (at.%) and α-Mg, respectively. In addition, grain boundaries of ZK60 are poorly defined because of incomplete recrystallization. The microstructure, however, becomes reasonably homogeneous after T5 heat treatment, and grain boundaries are clear in Fig. 2b, the grains grow up and show more global because of recrystallization behavior.

Figure 3 shows X-ray diffraction patterns of ZK60 and ZK60-T5 magnesium alloys. The peaks in the ZK60 magnesium alloy can be indexed as α-Mg and $MgZn_2$, and there are MgZn precipitates besides of α-Mg and $MgZn_2$ in ZK60-T5 magnesium alloy in Fig. 3b [18–20]. The references [18, 19] indicate that the aging precipitation process of ZK60 include GP zone and β' (MgZn), Sturkey and Clark [21] pointed out that the β' phase, which is similar to the laves phase ($MgZn_2$) in structure, is main precipitate in Mg–Zn alloys, β' is so steady that can be transformed to a equilibrium phase only through hundreds of hours aging treatment. Chun and Byrne [20] indicated that the strengthening mechanism of β' precipitates for ZK60 magnesium alloy is the cutting of β' precipitates by dislocations, rather than the bowing of dislocations between the precipitates [22], i.e. the mechanism of aging strengthening is shear mechanism; mechanical properties of ZK60 magnesium alloy can be improved by increasing density of β'. For ZK60-T5 magnesium alloy,

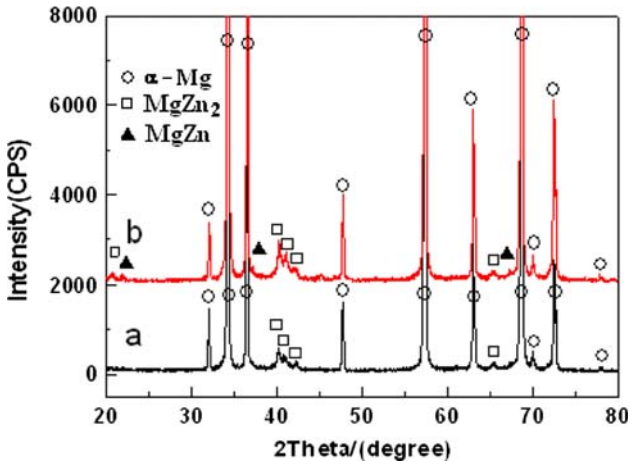

Fig. 3 XRD analysis of the high-strength magnesium alloy ZK60. (a) ZK60; (b) ZK60-T5

since it holds microstructure as dislocation and substructure similar to that of ZK60 magnesium alloy during T5 heat treatment, it is beneficial for the precipitation of β' becoming more homogeneous, smaller, and denser, and is beneficial to precipitation of β'.

Crystallographic textures ($\{0001\}$ pole figure and $\{10\bar{1}0\}$ pole figure) of ZK60 and ZK60-T5 are shown in Fig. 4. The basal planes are oriented predominantly parallel to the ED. As seen from Fig. 4, it is evident that $\{0001\}$ basal plane and $\langle 10\bar{1}0\rangle$ crystallographic direction in most grains are distributed parallel to the ED. That is, the ZK60 and ZK60-T5 magnesium alloys exhibits an ED// $\langle 10\bar{1}0\rangle$ fiber texture. Similar tendency of basal planes lying parallel to the ED after direct extrusion has been observed by other investigators [23–25] in other magnesium alloys. In addition, T5 heat treatment has a little effect on texture of ZK60 magnesium alloy; the pole figure intensity of ZK60-T5 magnesium alloy is slightly higher than that of ZK60 magnesium alloy.

Mechanical properties

Fourteen tensile specimens were tested under the initial strain rate of 5×10^{-4} s^{-1}. Table 3 shows the tensile properties of ZK60 and ZK60-T5 magnesium alloys. The tensile stress–strain curve determined is shown in Fig. 5. As seen from Table 3 and Fig. 5, in comparison to ZK60

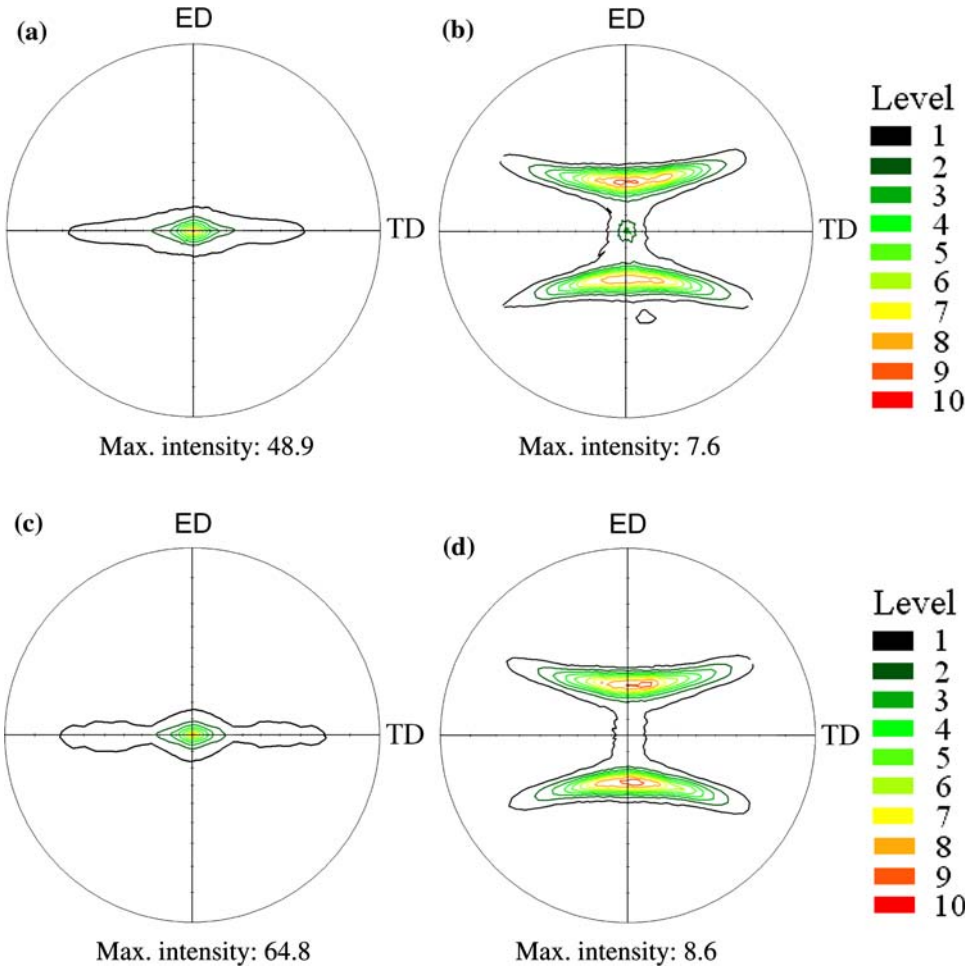

Fig. 4 $\{0001\}$ and $\{10\bar{1}0\}$ pole figures of ZK60 and ZK60-T5 magnesium alloys. **a** ZK60 $\{0001\}$; **b** ZK60 $\{10\bar{1}0\}$; **c** ZK60-T5 $\{0001\}$; **d** ZK60-T5 $\{10\bar{1}0\}$

Table 3 Tensile results on magnesium alloys ZK60 and ZK60-T5

Material	Testing direction	YS/MPa		UTS/MPa		EL (%)	
		$\bar{v}$	S	$\bar{v}$	S	$\bar{v}$	S
ZK60	ED	237	4.1	312	4.6	15.5	0.8
ZK60-T5	ED	273	4.4	329	3.2	16.5	0.9

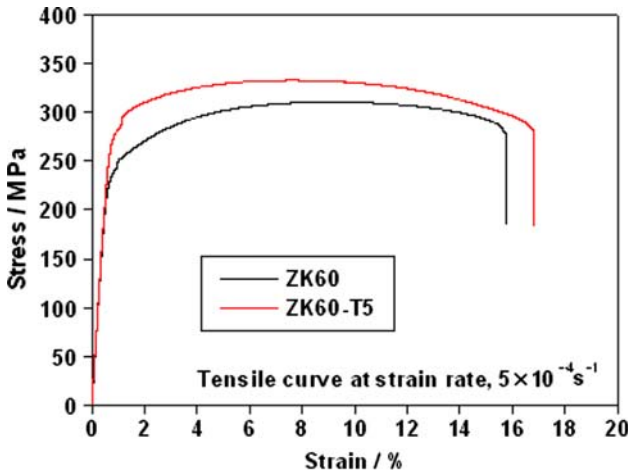

Fig. 5 Tensile stress–strain curve of ZK60 magnesium alloy tested at a strain rate of 5×10^{-4} s^{-1}

magnesium alloy, it can be seen that yield strength, ultimate tensile strength, and elongation of ZK60-T5 magnesium alloy increased by 15.2%, 5.4%, and 6.5%, respectively.

Factors that influence the tensile properties of ZK60 and ZK60-T5 magnesium alloys include the following: size and distribution of pores and/or inclusion particles, grain size, texture intensity, size, and distribution of $MgZn_2$ and MgZn precipitates. As remarked above, for ZK60 is a precipitation-strengthening magnesium alloy [18–20], the potential in yield strength, ultimate tensile strength, and elongation cannot be fully brought out unless the necessary artificial aging is performed; therefore, precipitation strengthening is the most important mechanism because of which the tensile properties of ZK60-T5 magnesium alloy are increased. It is well known that the $MgZn_2$ is the main strengthening phase in ZK60 alloy (see Fig. 3). Galiyev, Zhang, and co-workers [26, 27] reported that $MgZn_2$ and Zn_2Zr_3 phases might also be contained in the matrix. In addition, in comparison to 2ZK60 magnesium alloy, higher texture intensity (see Fig. 4) is also a main factor to improve the tensile properties of ZK60-T5 magnesium alloy [28].

The fracture surfaces of tensile specimens of ZK60 and ZK60-T5 magnesium alloys are shown in Fig. 6, which consist of voids with different sizes, shallow dimples, and some fractions of cleavage fractures; and the whole fracture surface inclines to the loading axis and is close to the plane with maximum shear force. In comparison to ZK60 magnesium alloy (see Fig. 6a), after T5 heat treatment, the cleavage planes decrease gradually and the plastic dimples increase greatly (see Fig. 6b). In general, the dimple is mainly caused by the existence of inclusions or second phases. It has been reported that the dimple size depends on the inclusion size [29]. The optical micrographs of ZK60 and ZK60-T5 magnesium alloys on the section parallel to the gage length confirm that the fracture surfaces of the tensile specimen are very bumpy and show a typical ductile failure (see Fig. 7). Voids form along the interface of the entrapped particles and matrix during tensile loading. They then coalesce and exhibit shallow dimples. When the matrix has inherently few particles, the cracks proceed in a trans-granular form and develop cleavage failure. It can be seen there are many slip bands near fracture surface in Fig. 7a, b, and density of slip bands decreases as the length of the fracture surface increases. Figure 7 also demonstrates banded structures, which are the typical structures of hot-extruded bar. Dimples shown on the fracture surface may also originate from the banded structure where slip bands and/or deformation twins intersect and generate micro-voids. These voids coalesce and provide potential sites for forming dimples during tensile loading. In addition, a few deformation twins are visible in the matrix near the fracture surface. In comparison to ZK60 magnesium alloy (see Fig. 7a), the optical micrograph of ZK60-T5 magnesium alloy has more regular and global crystal, which can deform evenly during tensile loading, whereas lots of precipitates of MgZn in the Mg matrix can also strengthen ZK60-T5 magnesium alloy by acting as barriers to the dislocation movement. Therefore, more persistent slip bands and deformation twinning are parallel in Fig. 7b.

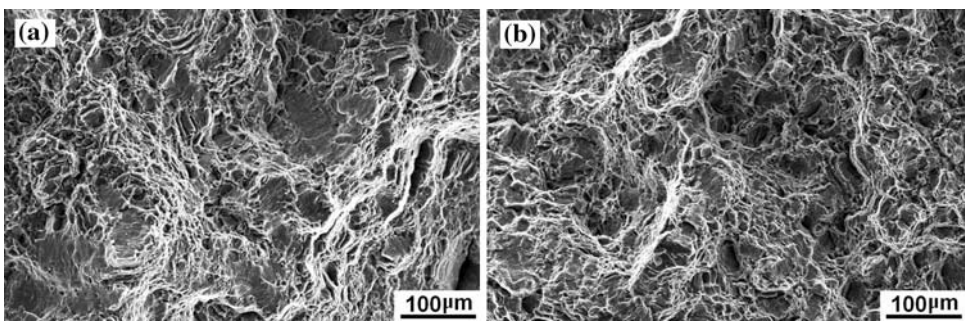

Fig. 6 Fracture surface of tensile specimen (SEM). **a** ZK60; **b** ZK60-T5

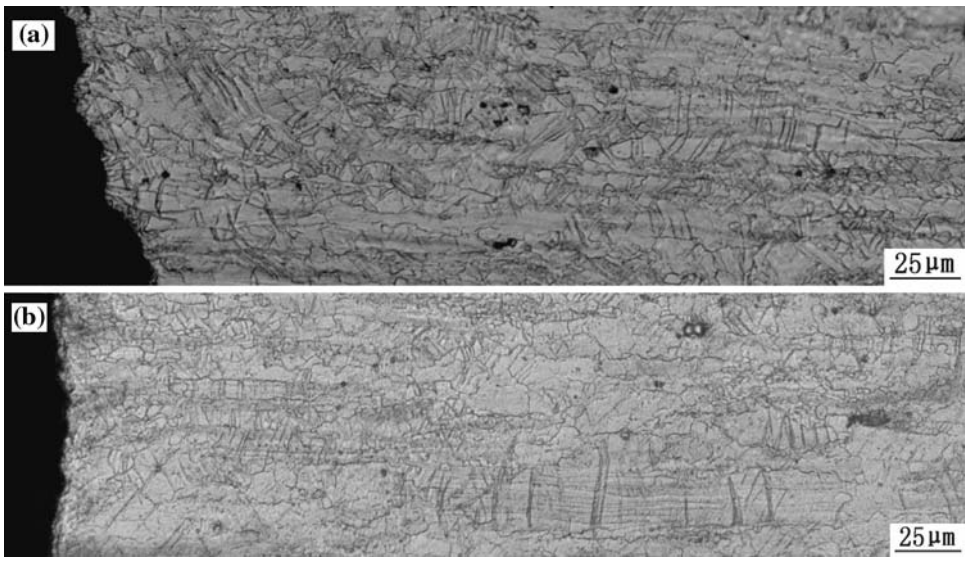

Fig. 7 Optical microstructures for sample sectioned in direction parallel to the gage length, indicating banded structures and the outline of the fracture surface. **a** ZK60; **b** ZK60-T5

High cycle fatigue properties

The *S–N* curves of ZK60 and ZK60-T5 magnesium alloys under rotating beam loading ($R = -1$) at a frequency of about 100 Hz in air are presented in Fig. 8. The fatigue strength (at 10^7 cycles) of ZK60 magnesium alloy is 140 MPa, while that of ZK60-T5 magnesium alloy is 150 MPa, i.e., the improvement of 7% in fatigue strength has been achieved. The fatigue ratio (σ_a/σ_b) for the investigated alloys are about 0.45 and 0.46, respectively, in agreement with the value for magnesium (0.25–0.5) reported in literature [30]. In addition, fatigue life of ZK60-T5 magnesium alloy is higher than that of ZK60 magnesium alloy, particularly, at the lower stress amplitude.

The distinction of the *S–N* curves and the fracture morphologies between ZK60 and ZK60-T5 magnesium alloys should be ascribed to the different microstructures, which will be discussed deeply as follows.

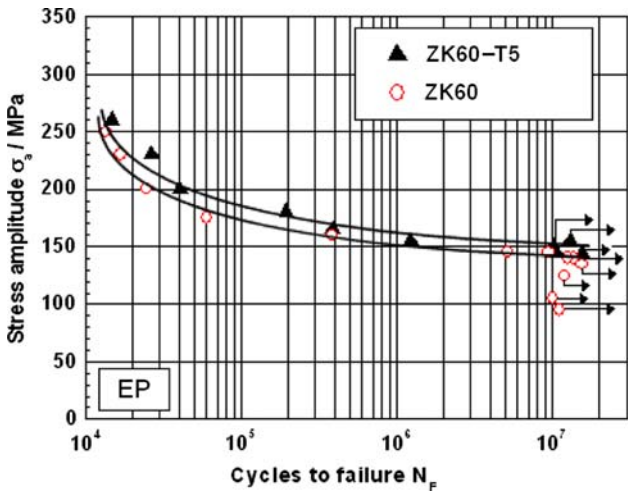

Fig. 8 *S–N* curve of ZK60 and ZK60-T5 under rotating beam loading in air ($R = -1$)

Fracture surfaces of ZK60 and ZK60-T5 fatigue specimens are shown in Fig. 9. It can be seen that fatigue cracks initiate on specimen surfaces (see Fig. 9a, c), since the surface experiences the maximum tension stress due to rotating beam loading fatigue. In addition, due to the lack of constraint in grains at free surface, the glided dislocations during deformation may result in a microscopically irregular surface, which makes the surface as a prevailing site for crack initiation. A close-up of fracture surface near crack nucleation area shows a typical cleavage feature, which consists of lots of lamellar cleavage planes (see Fig. 9b, d). This result indicates that the fatigue crack propagation is characterized by striation-like features coupled with secondary cracks along the cleavage plane in ZK60 and ZK60-T5 magnesium alloys at the beginning of propagation, opposite to tensile fracture, in which crack propagates by coalescence of dimples (see Fig. 6).

However, the main difference of fracture surface of ZK60 and ZK60-T5 magnesium alloys is in fatigue crack propagation zone, as seen from Fig. 9b, d, the fracture surface of ZK60-T5 magnesium alloy is rougher than that of ZK60 magnesium alloy, and has more cleavage planes, dimples and tear ridge. Comparison to ZK60 magnesium alloy (see Fig. 9a), ZK60-T5 magnesium alloy has more regular and global crystal, which can deform evenly during cyclic loading, meanwhile, dislocation mainly moves in basal plane which has lower strength, and the precipitates of MgZn in the Mg matrix will be the predominant barriers to the dislocation movement. The basal plane of the MgZn precipitate is perpendicular to the basal plane of the Mg matrix; however, the plane of the highest atomic density in the MgZn precipitate is $(2\bar{1}\bar{1}0)$ [20]. Thus dislocations in the Mg basal plane should cut through the MgZn precipitates, resulting in slip plane

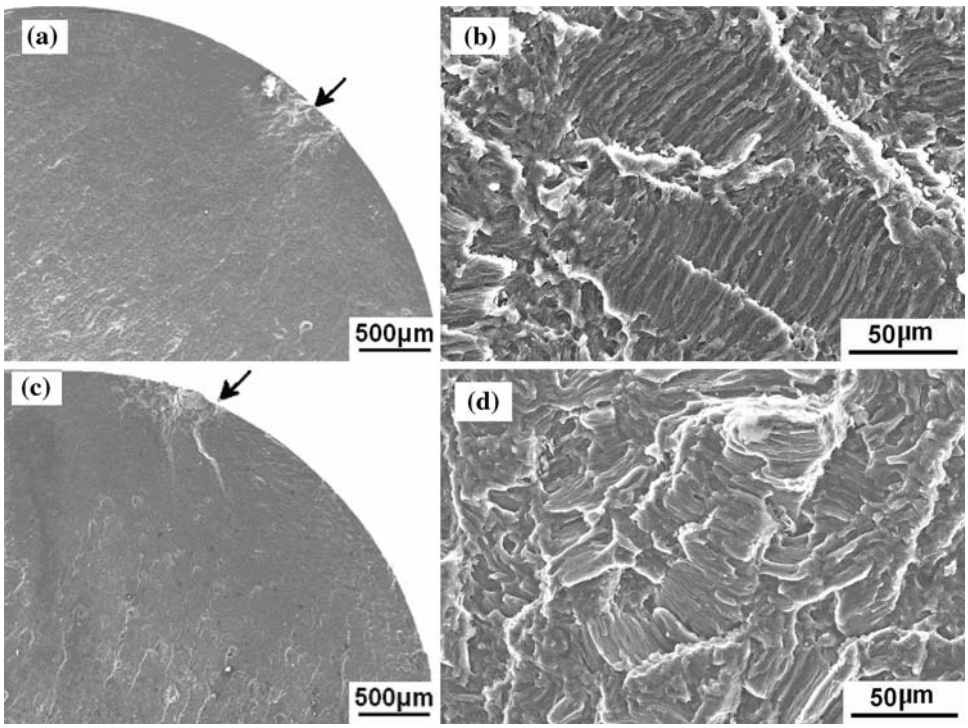

Fig. 9 Fatigue crack nucleation sites of ZK60 and ZK60-T5 alloys (SEM): **a** an overview of ZK60; **b** a close-up near crack initiation region of ZK60. **c** an overview of ZK60-T5; **d** a close-up near crack initiation region of ZK60-T5 (arrow indicates crack nucleation site)

produces partial strengthening and blocks dislocation movement. In addition, more regular and global crystals are more effective to blocks dislocation movement. Hence, higher fatigue strength in ZK60 magnesium alloy is induced after T5 heat treatment.

The result of LOM observations on a ZK60 specimen surface as detected by the replica method during fatigue at stress amplitude of 165 MPa is shown in Fig. 10. In order to examine the interaction between crack initiation and propagation behaviors and the microstructure of the specimen, the fatigue experiment was conducted on the specimen whose microstructure was pre-revealed by etching. As seen from Fig. 10, a crack initiates at the banded region that is equivalent to dark-banded layer in Fig. 2a, and in this region the crack path is straight, showing characteristic transgranular fracture. Then the fatigue crack propagates into the neighboring regions that are equivalent to light-banded layers in Fig. 2a, and in this region the path of fatigue crack growth is mainly intergranular. In addition, the crack propagated along the cleavage planes into the neighbouring grains after crossing over the grain boundary, which is consistent with the results of SEM observation on fracture surface (see Fig. 9a). The same phenomenon is also observed on ZK60-T5 specimen.

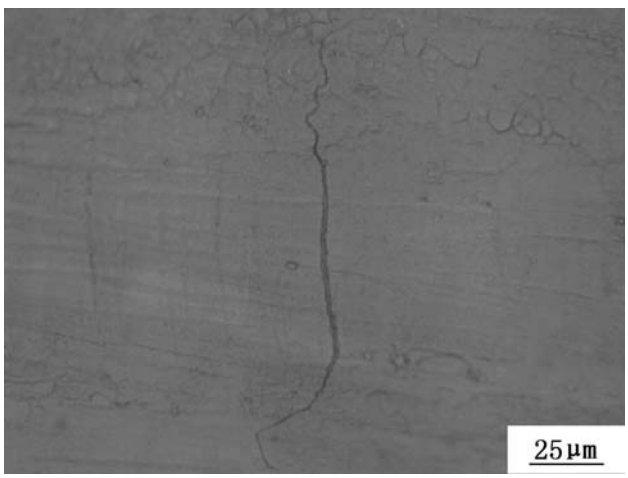

Fig. 10 LOM observation on the ZK60 specimen's surface as detected by the replica method during fatigue at stress amplitude of 165 MPa

Figure 11a, b shows the microstructures of ZK60 and ZK60-T5 magnesium alloys on the section parallel to the gage length below the fracture surface. Banded layers exist in a matrix of fatigue specimen near fracture surface that is mostly composed of fine grains. However, the banded layers located in the matrix of the tensile specimens are rich in slip bands and deformation twins (see Figs. 7 and 11). The phase transformation from the original banded layer to fine grains can be attributed to dynamic recrystallization due to cyclic loading. In deforming magnesium alloy, the sense of shear is that twinning is favored by compression [31]. In comparison to ZK60 magnesium alloy (see Fig. 11a), the optical micrograph of ZK60-T5 magnesium alloy has more regular and global crystal, which can deform evenly during cyclic loading, whereas lots of precipitates of MgZn in the Mg matrix can also strengthen ZK60-T5 magnesium alloy

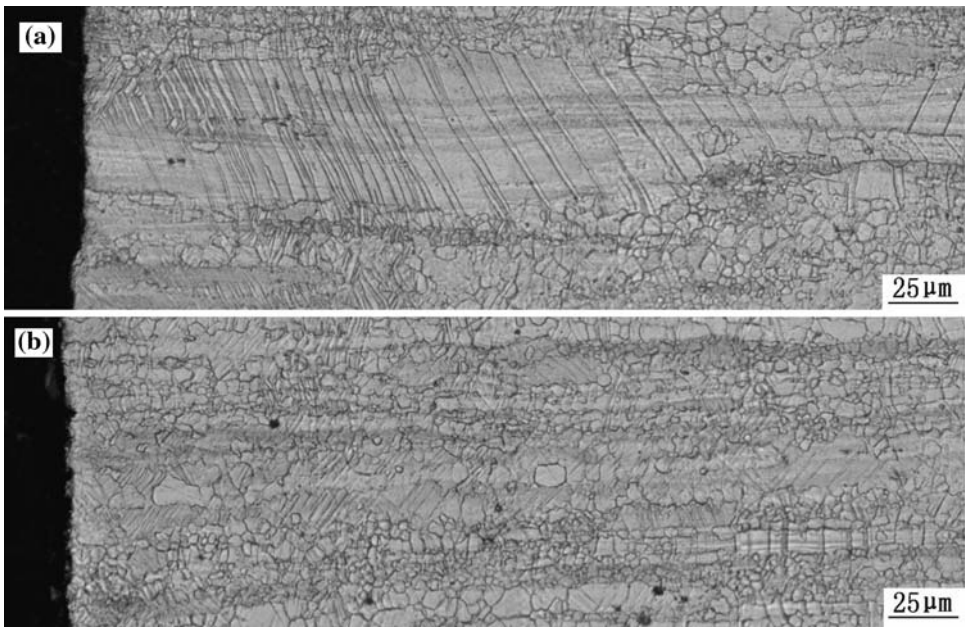

Fig. 11 Optical microstructures of matrix near the crack initiation of ZK60 and ZK60-T5 test bar subjected to **a** a stress amplitude, 160 MPa and which failed at 3.8×10^5 cycles; **b** a stress amplitude 175 MPa and which failed at 1.9×10^5 cycles; deformation twins are visible

through acting as barriers to the dislocation movement. Therefore, more persistent slip bands and deformation twinning are parallel in Fig. 11b.

Conclusions

Tensile and high cycle fatigue properties of hot-extruded ZK60 magnesium alloy have been investigated, in comparison to that of hot-extruded plus T5 heat-treated magnesium alloy ZK60 was which named as ZK60-T5. The following conclusions can be drawn:

- Obvious changes have taken place in microstructure and texture of ZK60 magnesium alloy after T5 heat treatment. Three-banded layers (corresponding to the A, B, and C compound) of ZK60 magnesium alloy in a plane parallel to the ED changed into two-banded layers (corresponding to the A and D compounds) of ZK60-T5 magnesium alloy. In comparison to ZK60 magnesium alloy, ZK60-T5 magnesium alloy has more regular and global grain crystal, and higher pole figure intensity of fiber texture.
- The yield strength, ultimate tensile strength, and elongation of ZK60 magnesium alloy are improved after T5 heat treatment.
- Fatigue strength of ZK60 magnesium alloy at $R = -1$ and 10^7 cycles is 140 MPa, while that of ZK60-T5 magnesium alloy is 150 MPa, which gives the fatigue ratio (σ_a/σ_b) for the investigated alloys as about 0.45 and 0.46, respectively. The improvement of 7% in fatigue strength has been achieved by T5 heat treatment. In addition, fatigue life of ZK60-T5 magnesium alloy is higher than that of ZK60 magnesium alloy, particularly, at the lower stress amplitude.
- The fatigue cracks of ZK60 and ZK60-T5 magnesium alloys initiate in dark-banded layer of specimen surface; a close-up of fracture surface near crack nucleation area shows a typical cleavage feature, which consists of lots of lamellar cleavage planes. The main difference of fracture surface of ZK60 and ZK60-T5 magnesium alloys is in fatigue crack propagation zone, where the fracture surface of ZK60-T5 magnesium alloy is rougher than that of ZK60 magnesium alloy, and has more cleavage planes, dimples, and tear ridge.

Acknowledgements This project is sponsored by National Ministry of Science and Technology (Grant No. 2007CB613703), Shanghai Pujiang Program (Grant No. 06PJ14062), and the Scientific Research Foundation for the Returned Overseas Chinese Scholars, State Education Ministry, ROC.

References

1. Yang Y, Liu YB (2008) Mater Charact 59:567
2. Luo A, Pekguleryuz MO (1994) J Mater Sci 29:5259. doi: 10.1007/BF01171534
3. Mordike BL, Ebert T (2001) Mater Sci Eng A 302:37
4. Luo AA (2002) JOM (J Met) 54(2):42
5. Luo AA (2005) SAE Trans-J Mater Manuf 114(5):411
6. Feng L, Yue W, Lihia C, Zheng L, Jiyang Z (2005) J Mater Sci 40(6):1529. doi:10.1007/s10853-005-0597-8
7. Zhou HT, Zhang ZD, Liu CM, Wang QW (2007) Mater Sci Eng A 445–446:1
8. Figueiredo RB, Langdon TG (2007) Mater Sci Eng A. doi: 10.1016/j.msea.2008.04.080
9. Lapovok R, Thomson PF, Cottam R, Estrin Y (2005) Mater Sci Eng A 410–411:390

10. Wang CY, Wu K, Zheng MY (2008) Mater Sci Eng A 487:495
11. Gray JE, Luan B (2002) J Alloys Compd 336:88
12. Unigovski Ya, Eliezer A, Abramov E, Snir Y, Gutman EM (2003) Mater Sci Eng A 360:132
13. He SM, Peng LM, Zeng XQ, Ding WJ, Zhu YP (2006) Mater Sci Eng A 433:175
14. Xie GM, Ma ZY, Geng L (2008) Mater Sci Eng A 486:49
15. Xu DK, Liu L, Xu YB, Han EH (2007) J Alloys Compd 431:107
16. Ishihara S, Nan ZY, Goshima T (2007) Mater Sci Eng A 468–470:214
17. Nan ZY, Ishihara S, McEvily AJ, Shibata H, Komano K (2007) Scripta Mater 56:649
18. Das SK, Chang CF (1992) Magnesium alloys and their applications[M]. FRG.DGM Internation Sgesellschaft, Manchester, p 487
19. Polmear IJ (1989) Light alloys: metallurgy of light metals[M], 2nd edn. Edward Arnold, London, p 210
20. Chun JS, Byrne JG (1969) J Mater Sci 4:861. doi:10.1007/BF00549777
21. Sturkey L, Clark JB (1959) J Inst Metal 88:177
22. Clark JB (1965) Acta Metall 13:1281
23. Kim WJ, Hong SI, Kim YS, Min SH, Jeong HT, Lee JD (2003) Acta Mater 51:3293
24. Hilpert M, Styczynski A, Kiese J, Wagner L (1998) In: Mordike BL, Kainer KU (eds) Magnesium alloys and their applicacation. Wiley-VCH, Weinheim, Frankfurt, Germany, p 319
25. Mukai T, Yamanoi M, Watanabe H, Higashi K (2001) Scripta Mater 45:89
26. Galiyev A, Kaibyshev R, Gottstein G (2001) Acta Mater 49:1199
27. Zhang SQ (1989) Acta Metall Sin 25(5):346; in Chinese
28. Duly D, Simon JP, Brechet Y (1995) Acta Metall Mater 43(1):101
29. Higashi K, Hirai Y, Ohnishi T (1985) Jpn J Inst Light Met 35:520
30. Ogarevic VV, Stephens RI (1990) Annu Rev Mater Sci 20:141
31. Reed-Hill RE, Abbaschian R (1994) Physical metallurgy principles, 3rd edn. PWS Publishing, Boston, p 194